Accurate Tissue Deformation Modelling Using a Kalman Filter and ADMM-based Projective Dynamics

Mehrnoosh Afshar[1], Jay Carriere[1], Hossein Rouhani[2], Tyler Meyer[3], Ron Sloboda[4], Siraj Husain[3], Nawaid Usmani[4], and Mahdi Tavakoli[1], *Senior Member, IEEE*

Abstract—In low-dose-rate permanent-seed (LDR-PS) brachytherapy, it is crucial to predict the movement of internal targets (planned radioactive seed locations) under the effect of external forces. Accurate prediction of the target's location is critical to precise seed implantation, and inaccurate seed implantation diminishes the effectiveness of radiotherapy. Therefore, developing a model to simulate the tissue dynamics is necessary. However, fully vision-based data-driven models to predict tissue dynamics are inapplicable to tasks, such as internal tissue deformation prediction, since these approaches can only capture geometrical changes detected by cameras. Therefore, a physics-based model capable of modelling the nonlinear mechanical properties of soft tissue in real-time is needed to simulate internal tissue dynamics. All physics-based models have model-reality mismatches due to unmodeled dynamics, which should be addressed. In this work, we propose the KF-ADMM method as a solution to compensate for unmodelled dynamic terms existing in the alternating direction method of multiplier (ADMM)-based projective dynamics tissue simulator through Kalman filtering. The ADMM-based projective dynamics is an open-loop tissue simulator in which the output (i.e., deformed tissue) is not compared with real tissue deformations, nor is the feedback used to update the estimation error. In contrast, closed-loop tissue simulators utilize feedback to improve the accuracy of the deformation estimation. Visual data can be incorporated into the open-loop tissue simulator by integrating a Kalman filter into the nonlinear tissue deformation simulator. This method provides accurate predictions of the location of inner tissue points with an error of around 0.8 mm. Experiments on a breast tissue phantom are performed to evaluate the efficacy of the proposed approach. According to the results, the accuracy of tissue deformation is enhanced by 52% on average, and the convergence rate is accelerated compared to an open-loop tissue simulator.

Index Terms—Breast brachytherapy, Kalman filtering, Medical robotics, Soft tissue simulator, ADMM-based Projective dynamic

[1]Mehrnoosh Afshar, Jay Carriere and Mahdi Tavakoli are with the Department of Electrical and Computer Engineering, University of Alberta, AB, Canada T6G 1H9. afsharbo@ualberta.ca, jtcarrie@ualberta.ca,mahdi.tavakoli@ualberta.ca
[2]Hossein Rouhani is with the Department of Mechanical Engineering, University of Alberta, AB, Canada T6G 1H9. hrouhani@ualberta.ca
[3]Tyler Meyer and Siraj Husain are with the Division of Radiation Oncology, Tom Baker Cancer Centre, 331 29th Street NW, Calgary, Alberta T2N 4N2. tyler.meyer@albertahealthservices.ca, siraj.husain@albertahealthservices.ca.
[4]Ron Sloboda and Nawaid Usmani are with the Department of Oncology, Cross Cancer Institute, 11560 University Avenue, Edmonton, AB, Canada, T6G 1Z2. nawaid.usmani@albertahealthservices.ca, ron.sloboda@albertahealthservices.ca.

I. INTRODUCTION

THE low-dose-rate permanent-seed (LDR-PS) brachytherapy has shown great potential for treating breast cancer by offering a reduction in treatment time and better cosmetic outcome compared with other breast cancer treatments [1]. LDR-PS brachytherapy is a cancer treatment that make use of radioactive seeds which are injected at pre-planned desired locations inside or around a tumour or seroma (hollowed-out tumour). The challenge in breast brachytherapy is that breast tissue deforms easily and excessively during the brachytherapy procedure. As the US probe is moved over the breast surface the pressure from the US probe will deform the breast and change the location of the internal planned seeds location (targets) during treatment. During breast surgeries, displacements of up to 7 mm are common in the target area [2], [3]. Implanting seeds off-target results in insufficient radio therapy and the risk of cancer recurrence. In this case, the surgeon must analyze 2D US images to estimate the target location and then carryout the insertion. Consequently, precise brachytherapy seed implantation depends heavily on the clinician's skill and is vulnerable to human error. Current brachytherapy procedures would greatly benefit from a solution to track the targets location intraoperatively. The desired target locations for seeds may not be recognizablein on US images which usually have much noise and artifacts and where various targets are difficult to discern based on image characteristics [4]. Target tracking for breast brachytherapy can be achieved by using a patient-specific tissue deformation model.

Current tissue deformation models can be divided into three categories; 1) fully physics-based models, 2) end-to-end data-driven models, and 3) hybrid models, combining physics-based models with real deformation data. In the category of physics-based tissue simulators, the challenge is to address the trade-off between accuracy and computation time [5]; for many application in surgical robotics a real-time and accurate tissue simulator is required. Finite Element Methods (FEM) are widely used to simulate nonlinear and complicated mechanical behavior of tissue; however, they are computationally expensive at the moment to be used for real-time applications [6]. Numerous studies have applied model order reduction methods to FEM to enhance their computational

performance. The reduced order model FEMs are obtained via a substantial pre-operative calculation [7]. Neural networks can simulate any nonlinear functions in real-time [8], [9]. Mendizabal et al. in [10] proposed a method to estimate the deformation of breast tissue under US probe pressure using a U-net network trained from synthetic FEM simulations. As the neural network model is trained using FEM simulations, there may be a mismatch between the real situation and the model because it does not use real data. The neural network model is simply a faster version of the physics-based model. Furthermore, generating synthetic data sets and neural network training is time-consuming. Many studies simplified accurate models for a real-time solver in order to meet simulation speed requirements, however, this simplification decreases the model accuracy to some extent such as Mass Spring Models (MSMs) [11]. The proposed modifications to MSM which tried to simulate nonlinear properties of biological tissue such as viscoelasticity and incomprehensibility still fail to capture the true nonlinear force-displacement relationship of biological tissue [12], [13].

Position-based dynamics (PBD) methods, that are widely used to simulate object deformation in real-time for computer graphics applications, has recently been utilized to develop surgical simulators [14]. In PBD, an object is simulated as a grid of particles whose positions are derived from rigid body motion equations under geometric constraints [15]. A study by Tagliabue et al. [16] used PBD to predict the position of breast tumors in response to pressures from US scanning. Because the constraints in PBD are geometric, it does not reflect the mechanical characteristics of tissue. Therefore, the reported tumor localization error in [16] is extremely large for medical applications and it is about 5mm. The authors in [17] proposed the projective dynamics method that can impose a wider range of constraints than geometric constraints in the PBD. In this study, simple strain potential energy functions are also used as constraints. In [18], a generalization of the projective dynamics method is presented that permits solving any nonlinear constraint. In this method, the alternating direction method of multiplier (ADMM) is used as the optimizer. As opposed to the usual optimizers, ADMM allows computations to be parallelized, making it a viable choice for simulations that occur in real-time. So far, this method has not been implemented to model complicated mechanical characteristics such as hyperelasticity and viscoelasticity in soft tissue. In summary, there is a mismatch between physical-based tissue simulators and reality resulting from the simplifications made to keep up with speed requirements. It is critical to address this mismatch when it comes to surgical applications.

To resolve the problem of simulation-reality mismatch, researchers have tried to model end-to-end behaviour of tissue using deep learning models that are trained based on visual information from deformed tissue as the primary source of information during operation [19], [20]. The main limitation of relying only on exterior visual perception is that it cannot provide information on the internal structure of tissues/organs [21].

The third category, hybrid simulators, compensate for model mismatch of physics-based simulators with the aid of real data.

For surgical applications, real-time data from the deformed tissue captured by visual sensors can provide a good basis for updating an existing inaccurate physics-based model [21]. Thus, it is beneficial to have a visual perception of the tissue and to track its deformation in real-time in order to update the physics-based model accordingly. Liu et al. in [21] developed a real-time, online registration method that incorporates 3D visual perception and PBD simulation. As the PBD method are not capable of predicting tissue deformation, in [21], the visual data from the tissue surface is integrated with the PBD simulation to enable accurate prediction of tissue deformation. However, in [21], the proposed framework has not been tested for the ability to predict deformations of the internal points of the tissues. As PBD is developed based on geometric constraints rather than mechanical properties of the tissue, it will not be able to simulate the internal deformation of the tissue accurately.

To the best knowledge of the author, hybrid simulators for tissue deformation estimation are still in their infancy. While this type of tissue deformation model is the key to eliminate the mismatch between the simulator and reality, and also maintain a real-time framework. Bayesian filtering methods are a great tool for bridging the gap between simulation and reality. A Bayesian filter can infer from real observations in a data-efficient manner and leverage simulation as a source of prior knowledge. However, implementing Bayesian filtering methods on deformable tissue is challenging considering the non-linearity and high-dimensionality of the problem. Currently, the literature lacks the integration of a Bayesian filter into physics-based tissue simulator, which is the main goal of this paper.

A. Objective and Contributions

In this work, the objective is to bridge the gap between real-time physics-based tissue simulators and reality by integrating a few positional data from the tissue surface into the physics-based tissue simulator through the context of Bayesian filtering. ADMM-based PD is chosen as real-time physics-based model of tissue deformation due to the fact that it solves nonlinear tissue dynamic equations in an optimization-based framework which is paralliazable.Kalman filter (KF) is chosen from the Bayesian filter methods since KF is the optimal estimator in term of minimum least square error for linear systems. Considering the optimality of KF for linear systems and its manageable computational burdens with respect to other variant of KF, like extend KF (EKF), KF is chosen as the estimator method. In order to make nonlinear dynamics equations compatible with KF structure, the nonlinearity occurring in the tissue dynamics equations is transferred to the input term, resulting in a linear state-space model with a fixed transition matrix. As a result, the transition matrix does not need to be recalculated at each step, which significantly reduces the computation burden of the entire algorithm. The proposed framework is called KF-ADMM. In summary, the contributions of this study are as follows:

1) Nonlinear tissue dynamics equations are converted into a linear state-space model with a fixed transition matrix

and nonlinear inputs. In this way, the linear KF can be used which saves a lot of computations.

2) Parallel implementation of ADMM-based PD and matrix multiplications associated with KF increase the KF-ADMM speed.

3) This method does not require observation of the entire deformable tissue, and a few discrete measurements on the surface are sufficient for increasing accuracy.

4) Integration of the Kalman filter significantly improves the accuracy of the deformation estimation and the convergence rate of the open-loop simulator.

5) The presented framework can be extended to a broader range of surgical applications in which visual perception of the tissue deformation is available.

The rest of the paper is organized as follows. The biomechanical solver and material model will be presented in Section II. The state-space model of the biomechanical solver will be derived and the development of the Kalman filter based on the derived equations will be elaborated in Section III. In Section IV, the efficacy of the proposed framework in tissue deformation prediction will be evaluated experimentally, and a conclusion in Section V will complete the paper.

II. TISSUE MODELLING

In this section, the ADMM-based projective dynamics method is explained, and the mechanical material model that is selected to represent tissue behavior is elaborated.

A. Dynamics of Tissue Deformation

Objects are discretized using elements (triangles in 2D, tetrahedra in 3D) and lumped masses are integrated into the node of the elements. The Degree of Freedom (DoF) of the dynamic system is equal to the number of nodes used to discretize the tissue domain multiplied by three in the case of 3D simulation. Based on the work in [18], the position of these lumped masses (i.e., Dof of the system) can be calculated by solving the following optimization problem

$$\mathbf{x} = \arg\min_{\mathbf{x}} \left(\frac{1}{2\Delta t^2} \|\mathbf{x} - \tilde{\mathbf{x}}\|_{\mathbf{M}}^2 + \mathbf{U}(\mathbf{x}) \right) \quad (1)$$

where,

$$\tilde{\mathbf{x}} = \mathbf{x} + \mathbf{v}\Delta t + \mathbf{M}^{-1}\mathbf{F}_{\mathbf{ext}}\Delta t^2 \quad (2)$$

determines the position of lumped masses in the absence of internal forces. $\mathbf{M}$ is the matrix of lumped masses and $\mathbf{F}_{\text{int}}$ is the external forces acting on each lumped mass. $\mathbf{U}$ is the potential function that determines the internal relations between nodes. It is selected to be strain energy function, thus the internal forces are calculated as the gradient of strain energy function $\mathbf{F}_{\text{int}} = -\nabla\mathbf{U}(\mathbf{x})$. In the above, $\mathbf{v}$ is the velocity of each lumped mass. Δt is the sampling time chosen to simulate the tissue dynamics and $\|\mathbf{x}\|_{\mathrm{M}} = \sqrt{\mathbf{x}^T \mathbf{M} \mathbf{x}}$. (1) is a high-dimensional nonlinear optimization problem and it is not possible to be solved in a time-efficient manner. To overcome this issue a solution, which is suggested in [18], is to use the alternating direction method of multipliers optimizer (ADMM) which in general is an optimizer for distributed systems.

B. ADMM Optimizer

The basics of ADMM is described in this section. The ADMM is a method to solve optimization problems having the form [22]

$$\begin{aligned} \arg\min_{\mathbf{x},\,\mathbf{z}} \quad & \mathbf{h}(\mathbf{x}) + \mathbf{g}(\mathbf{z}) \\ \text{s.t.} \quad & \mathbf{Ax} + \mathbf{Bz} = \mathbf{C} \end{aligned} \quad (3)$$

where $\mathbf{h}$ and $\mathbf{g}$ are general cost functions subjected to a set of linear constraints, and $\mathbf{A}$ and $\mathbf{B}$ are general constant matrices. The algorithm works by introducing a dual variable $\mathbf{u}$ and iterating the following update rules

$$\begin{aligned} \mathbf{x}_{n+1} &= \arg\min_{\mathbf{x}} \left(\mathbf{h}(\mathbf{x}) + \frac{\rho}{2} \|\mathbf{Ax} + \mathbf{Bz}_n - \mathbf{C} + \mathbf{u}_n\|^2 \right) \\ \mathbf{z}_{n+1} &= \arg\min_{\mathbf{z}} \left(\mathbf{g}(\mathbf{z}) + \frac{\rho}{2} \|\mathbf{Ax}_{n+1} + \mathbf{Bz} - \mathbf{C} + \mathbf{u}_n\|^2 \right) \\ \mathbf{u}_{n+1} &= \mathbf{u}_n + (\mathbf{Ax}_{n+1} + \mathbf{Bz}_{n+1} - \mathbf{C}) \end{aligned}$$

$$(4)$$

Here, n indicates the number of iterations until the ADMM converges, and ρ is a weighting scalar.

C. ADMM Implementation For Tissue Deformation Calculation

The strain energy deformation $\mathbf{U}$ is a function of the gradient deformation matrix (explained thoroughly in Section II-D). A vector composed of the elements of gradient deformation matrices associated with mesh elements can be introduced into (1) as a new variable denoted by $\mathbf{z}$. The condition $\mathbf{z} = \mathbf{Dx}$ is satisfied at each converged solution of (1). In fact, matrix $\mathbf{D}$ transforms $\mathbf{x}$ variables to the gradient deformation matrix space. Therefore, (1) can be reformulated as

$$\begin{aligned} \arg\min_{\mathbf{x},\mathbf{z}} \left(\frac{1}{2\Delta t^2} \|\mathbf{x} - \tilde{\mathbf{x}}\|_{\mathbf{M}}^2 + \mathbf{U}(\mathbf{z}) \right) \\ \text{s.t.} \quad \mathbf{W}(\mathbf{Dx} - \mathbf{z}) = \mathbf{0} \end{aligned} \quad (5)$$

where $\mathbf{W}$ is a weighting matrix. By comparing (1) and (5), the functions and matrices can be chosen as

$$\begin{aligned} \mathbf{h}(\mathbf{x}) &= \frac{1}{2\Delta t^2} \|\mathbf{x} - \tilde{\mathbf{x}}\|_{\mathbf{M}}^2, \quad \mathbf{g}(\mathbf{z}) = \mathbf{U}(\mathbf{z}) \\ \mathbf{A} &= \mathbf{WD}, \quad \mathbf{B} = -\mathbf{W}, \quad \mathbf{C} = 0 \end{aligned} \quad (6)$$

By substituting (6) into (4), the update rules for the tissue deformation dynamics problem can be obtained as

$$\begin{aligned} \mathbf{x}_{n+1} &= \arg\min_{\mathbf{x}} \left(\frac{1}{2\Delta t^2} \|\mathbf{x} - \tilde{\mathbf{x}}\|_M^2 + \frac{1}{2} \|\mathbf{W}(\mathbf{Dx} - \mathbf{z}_n + \mathbf{u}_n)\|^2 \right) \\ &= (\mathbf{M} + \Delta t^2 \mathbf{D}^T \mathbf{W}^T \mathbf{WD})^{-1} \\ &\quad (\mathbf{M}\tilde{\mathbf{x}} + \Delta t^2 \mathbf{D}^T \mathbf{W}^T \mathbf{W}(\mathbf{z}_n - \mathbf{u}_n)) \end{aligned} \quad (7)$$

$$\mathbf{z}_{n+1} = \arg\min_{\mathbf{z}} \left(\mathbf{U}(\mathbf{z}) + \frac{1}{2} \|\mathbf{W}(\mathbf{Dx}_{n+1} - \mathbf{z} + \mathbf{u}_n)\|^2 \right) \quad (8)$$

$$\mathbf{u}_{n+1} = \mathbf{u}_n + \mathbf{Dx}_{n+1} - \mathbf{z}_{n+1} \quad (9)$$

Since matrices in (7) are fixed and can be precalculated, so the update rule for $\mathbf{x}$ variable is computationally fast.

The power of the ADMM optimizer is that (8) can be solved for each element separately; therefore, the procedure can be implemented in parallel on GPU or multi-core CPU. For

each strain energy function associated with each element, the following optimization problem should be solved separately:

$$\mathbf{z}_{i,n+1} = \arg\min_{\mathbf{z}_i} \left(\mathbf{U}_i(\mathbf{z}_i) + \tfrac{1}{2} \|\mathbf{W}_i(\mathbf{D}_i \mathbf{x}_{n+1} - \mathbf{z}_i + \mathbf{u}_{i,n})\|^2 \right)$$
$$\mathbf{u}_{i,n+1} = \mathbf{u}_{i,n} + \mathbf{D}_i \mathbf{x}_{n+1} - \mathbf{z}_{i,n+1}$$
(10)

Here, i refers to the element number, and $\mathbf{z_i}$ is a vector containing elements of the gradient deformation matrix associated with element i. After updating variable $\mathbf{z_i}$ and $\mathbf{u_i}$ associated with individual elements separately, the global vector of $\mathbf{z}$ and $\mathbf{u}$ are updated and used to update the position vector $\mathbf{x}$ using (7). For more details about the implementation of ADMM, an interested reader should refer to [18].

D. Material Model

In this section, the $\mathbf{U}_i(\mathbf{z_i})$ that is used to solve the optimization problem in (10) is explained. Several material models exist to describe the hyperelastic behaviour of tissue including Neo-Hookean, Ogden, Mooney-Rivlin, and Arruda-Boyce models [23]. The Neo-Hookean model is the most relevant, and the most used, model for modelling breast tissue [24]. In this paper, Neo-Hookean material model is used to model breast tissue. The strain energy function of a Neo-Hookean material is given by [25]

$$\Psi = \frac{\mu}{2}\left(\overline{\mathbf{I}_1} - 3\right) + \frac{\kappa}{2}(\mathbf{J} - 1)^2$$
(11)

where $\mathbf{I}_3 = \det(\mathbf{C})$, $\mathbf{J} = \frac{1}{2}\mathbf{I}_3$, $\overline{\mathbf{C}} = \mathbf{J}^{-2/3}\mathbf{C}$ and $\overline{\mathbf{I}_1} = \text{tr}(\overline{\mathbf{C}})$. $\mathbf{C}$ is the right Cauchy–Green deformation tensor, obtained by $\mathbf{C} = \mathbf{F}^\top\mathbf{F}$, and $\mathbf{F}$ is the deformation gradient matrix. Material constants are $\mu = \frac{E}{2(1+v)}$, and $\kappa = \frac{E}{3(1-2v)}$, in which E is Young's modulus and v is Poisson's ratio. The strain energy of each element can be calculated using $U_i = \Psi_i \mathbf{V}_i$, where $\mathbf{V}_i$ is the initial volume of the element and Ψ_i is the value of the strain energy density function measuring element's deformation. $\mathbf{U}_i$ is used in (10) to update $\mathbf{z}_i$ value for each element.

III. MODEL REGISTRATION VIA THE PROPOSED KF-ADMM METHOD

First, the derivation of state-space equations of the tissue simulator is explained, and then the Kalman filter is integrated into the deformable objects modeling algorithm.

A. State-Space Model

By substituting (2) into (7) and rearranging the terms, (7) is transformed into a discrete dynamic model with linear transition matrix and nonlinear input part, as shown below:

$$\mathbf{x}_{n+1} = \left(\mathbf{M} + \Delta t^2 \mathbf{D}^T \mathbf{W}^T \mathbf{W}\mathbf{D}\right)^{-1} \left(2\mathbf{M}\mathbf{x}_n - \mathbf{M}\mathbf{x}_{n-1} + \right.$$
$$\left. \mathbf{F}^n_{\mathbf{ext}}\Delta t^2 + \Delta t^2 \mathbf{D}^T \mathbf{W}^T \mathbf{W}(\mathbf{z}_n - \mathbf{u}_n)\right)$$
(12)

The following discrete state-space equation for the system of equations (12), and (10) by considering the augmented state vector, $\mathbf{X}_{n+1} = \begin{bmatrix} \mathbf{x}_{n+1} \\ \mathbf{x}_n \end{bmatrix}$, can be considered:

$$\mathbf{X}_n = \begin{bmatrix} \mathbb{A} & \mathbb{B} \\ I & 0 \end{bmatrix} \mathbf{X}_{n-1} + \begin{bmatrix} \mathbb{H}(\mathbf{U}_n) \\ 0 \end{bmatrix}$$

$$\mathbf{U}_{n+1} = \begin{bmatrix} \mathbf{z}_{n+1} \\ \mathbf{u}_{n+1} \\ \mathbf{F_{ext,n+1}} \end{bmatrix} = \begin{bmatrix} \mathbf{f}(\mathbf{x}_{n+1}, \mathbf{u}_n) \\ \mathbf{u}_n + \mathbf{g}(\mathbf{x}_{n+1}, \mathbf{z}_{n+1}) \\ \mathbf{F_{ext,n+1}} \end{bmatrix}$$
(13)

In the above,

$$\mathbb{A} = 2\left(\mathbf{M} + \Delta t^2 \mathbf{D}^\top \mathbf{W}^T \mathbf{W}\mathbf{D}\right)^{-1}\mathbf{M}$$
$$\mathbb{B} = -\left(\mathbf{M} + \Delta t^2 \mathbf{D}^\top \mathbf{W}^T \mathbf{W}\mathbf{D}\right)^{-1}\mathbf{M}$$
$$\mathbb{H} = \left(\mathbf{M} + \Delta t^2 \mathbf{D}^T \mathbf{W}^T \mathbf{W}\mathbf{D}\right)^{-1}$$
$$\left(-\mathbf{M}\mathbf{x}^{n-1} + \mathbf{F_{ext,n}}\Delta t^2 + \Delta t^2 \mathbf{D}^T \mathbf{W}^T \mathbf{W}(\mathbf{z}_n - \mathbf{u}_n)\right)$$
$$\mathbf{f}(\mathbf{x}_{n+1}, \mathbf{u}_n) = \arg\min_{\mathbf{z}} \left(\mathbf{U}(\mathbf{z}) + \tfrac{1}{2}\|\mathbf{W}(\mathbf{D}\mathbf{x}_{n+1} - \mathbf{z} + \mathbf{u}_n)\|^2\right)$$
$$\mathbf{g}(\mathbf{x}_{n+1}, \mathbf{z}_{n+1}) = \mathbf{D}\mathbf{X}_{n+1} - \mathbf{z}_{n+1}$$
(14)

Due to the fact that the matrix $\mathbb{A}$ is built upon matrix $\mathbf{D}$, which maps the nodes' coordinates represented in the global framework into element representation, the matrix contains information about the mesh structure. The first line of the equation in (13), which represents the state evolution of the system, can be expressed in the general form of discrete dynamic systems with uncertainties as follows:

$$\mathbf{X}_{n+1} = \mathbb{S}\mathbf{X}_n + \mathbb{U} + \mathbf{w}_n$$
$$\mathbf{y}_n = \mathbb{C}\mathbf{X}_n + \mathbf{v}_n$$
(15)

Here, the first equation presents the state evolution model, and the second line shows the relationship between sensor measurements and the state variables. The process noise $\mathbf{w}_n$ and measurement noise $\mathbf{v}_n$ are white, zero-mean, and uncorrelated with known covariance matrices Q_n and R_n respectively. In this work, inaccuracy in the models is modeled as white noise.

B. Kalman Filter Integration

In summary, Kalman Filter (KF) provides a recursive method for estimating the state of a dynamic system when the system is noisy by estimating both the state vector and the error covariance matrix simultaneously at each iteration step. The KF approach improves the accuracy of state variable estimation by combining two sources of information, mathematical model and measurements. With this study, the aim is to estimate the position of internal points (in this case, the state vector of the system) using an imprecise biomechanical model. To improve the accuracy of the model, partial measurements of the tissue surface are used to compensate for model inaccuracies. As a result, the KF is an appropriate solution for the problem.

KF consists of two stages: prediction and update. KF provides a recursive method of estimating the state of a dynamic system in the presence of noise by simultaneously estimating and updating both the state vector ($\mathbf{x}_n$) and the error covariance matrix (Σ_n) at time step n.

A multivariable Gaussian distribution with mean vector and covariance matrix can be used for representing both the prior probability distribution (i.e., prediction step) and the posterior probability distribution (i.e., update step) of state vector. The prior mean vector and covariance matrix are denoted by μ'_n and Σ'_n respectively. Similarly, the posterior mean vector and covariance matrix are denoted by $\hat{\mu}_n$ and $\hat{\Sigma}_n$ respectively.

At the prediction step, the prior quantities are calculated using (16) for the discrete system of (15)

$$\begin{aligned} \mu'_n &= \mathbb{S}\hat{\mu}_{n-1} + \mathbb{U} \\ \boldsymbol{\Sigma}'_n &= \mathbb{S}\hat{\boldsymbol{\Sigma}}_{n-1}\mathbb{S}^T + \mathbf{Q}_{n-1} \end{aligned} \tag{16}$$

In the update step, μ'_n and Σ'_n are updated by incorporating the new sensor information $\mathbf{y}_n$ to the estimations obtained in the prediction step for $\mathbf{x}_n$. The final equations for finding $\hat{\mu}_n$ and $\hat{\Sigma}_n$ are given in (17)

$$\begin{aligned} \hat{\mu}_n &= \mu'_n + \mathbb{K}_n(\mathbf{y}_n - \hat{\mathbf{y}}_n) \\ \mathbb{K}_n &= \boldsymbol{\Sigma}'_n\mathbb{C}^T(\mathbb{C}\boldsymbol{\Sigma}'_n\mathbb{C}^T + \mathbf{R}_n)^{-1} \\ \hat{\mathbf{y}}_n &= \mathbb{C}\mu'_k \\ \hat{\boldsymbol{\Sigma}}_n &= \boldsymbol{\Sigma}'_n - \mathbb{K}_n\mathbb{C}\boldsymbol{\Sigma}'_n \end{aligned} \tag{17}$$

where $\mathbb{K}_n$ is called the Kalman gain matrix at time step n.

The output of the open-loop tissue simulator algorithm, (the output of (12)), is the prior estimation of the state vector, μ'_n. The posterior estimation of the state vector is calculated using (18)

$$\begin{aligned} \mathbf{x}_{n+1} &= \left(\mathbf{M} + \Delta t^2 \mathbf{D}^T\mathbf{W}^T\mathbf{W}\mathbf{D}\right)^{-1} (2\mathbf{M}\mathbf{x}_n - \mathbf{M}\mathbf{x}_{n-1} + \\ &\quad \mathbf{F}_{\mathbf{ext,n}}\Delta t^2 + \Delta t^2\mathbf{D}^T\mathbf{W}^T\mathbf{W}\left(\mathbf{z}_n - \mathbf{u}_n\right)) \\ &\quad + \mathbb{K}_n\left(\mathbf{y}_n - \hat{\mathbf{y}}_n\right) \end{aligned} \tag{18}$$

In case that $\mathbf{F}_{\mathbf{ext}}$ is not available and only the displacement of engaged nodes with actuator, $x_{actuator}$, are available, (18) can be re-written as

$$\begin{aligned} \mathbf{x}_{n+1} &= \left(\mathbf{M} + \Delta t^2\mathbf{D}^T\mathbf{W}^T\mathbf{W}\mathbf{D}\right)^{-1} \\ &\quad \left(\mathbf{M}\tilde{\mathbf{x}} + \Delta t^2\mathbf{D}^T\mathbf{W}^T\mathbf{W}\left(\mathbf{z}_n - \mathbf{u}_n\right)\right) + \mathbb{K}_n\left(\mathbf{y}_n - \hat{\mathbf{y}}_n\right) \end{aligned} \tag{19}$$

where,

$$\begin{aligned} \tilde{\mathbf{x}} &= \mathbf{x} + \mathbf{v}\Delta t \\ \tilde{x}_i &= \mathbf{x}_{\mathbf{actuator,i}} \end{aligned} \tag{20}$$

(10), (17), and (18) in case that $\mathbf{F}_{\mathbf{ext,n}}$ is available or (19) for situation that $\mathbf{x}_{\mathbf{actuator}}$ is available, form the new KF-ADMM method, which is elaborated in algorithm 1. In this algorithm, for tetrahedral elements, (10) is solved in parallel. In the second step, the Kalman gain is calculated using (17). Then, the real positional data of the surface nodes are obtained from the markers and are transformed into the simulation coordinate system. In the end, using these data and (18) or (19), the state vector of the system is calculated.

The block diagram of the proposed KF-ADMM method is elaborated in Fig. 1. In the open-loop simulator, actuator displacements act as an input, and at the same time, these displacements deform tissue in the real experimental setup. The open-loop simulator output and measured surface points from the experimental setup are inputs to the Kalman filter, which refines the mesh node positions according to the posi-

---

Algorithm 1: The proposed deformation modelling algorithm

Input: Optical marker data y, Actuator Movements $\mathbf{x}_{\mathbf{actuator}}$ or Actuator Forces $\mathbf{F}_{\mathbf{ext}}$.

1 **while** $n \leq N$ **do**
2    $\mathbf{y}_n \leftarrow$ Read Marker data
3   **for** *Each Tetrahedral Element* **do**
4      $\mathbf{z}_{i,n+1} = \arg\min_{\mathbf{z}_i}\left(\mathbf{U}_i\left(\mathbf{z}_i\right) + \frac{1}{2}\left\|\mathbf{W}_i\left(\mathbf{D}_i\mathbf{x}_{n+1} - \mathbf{z}_i + \mathbf{u}_{i,n}\right)\right\|^2\right)$
     $\mathbf{u}_{i,n+1} = \mathbf{u}_{i,n} + \mathbf{D}_i\mathbf{x}_{n+1} - \mathbf{z}_{i,n+1}$ (10)
5   **end**
6
7   Calculate Kalman Filter Gain
8    $\boldsymbol{\Sigma}'_n = \mathbb{A}\hat{\boldsymbol{\Sigma}}_{n-1}\mathbb{A}^T + \mathbf{Q}_{n-1}$
9    $\mathbb{K}_n = \boldsymbol{\Sigma}'_n\mathbb{C}^T(\mathbb{C}\boldsymbol{\Sigma}'_n\mathbb{C}^T + \mathbf{R}_n)^{-1}$
10    $\hat{\boldsymbol{\Sigma}}_n = $
     $\boldsymbol{\Sigma}'_n - \mathbb{K}_n\mathbb{C}\boldsymbol{\Sigma}'_n$ (17)
11   Update Sate Vector
12   **if** $\mathbf{F}_{\mathbf{ext,n}}$ *is available* **then**
13      $\mathbf{x}_{n+1} = \left(\mathbf{M} + \Delta t^2\mathbf{D}^T\mathbf{W}^T\mathbf{W}\mathbf{D}\right)^{-1} (2\mathbf{M}\mathbf{x}_n - \mathbf{M}\mathbf{x}_{n-1} +$
     $\mathbf{F}_{\mathbf{ext,n}}\Delta t^2 + \Delta t^2\mathbf{D}^T\mathbf{W}^T\mathbf{W}\left(\mathbf{z}_n - \mathbf{u}_n\right))$
     $+ \mathbb{K}_n\left(\mathbf{y}_n - \hat{\mathbf{y}}_n\right)$ (18)
14   **end**
15   **if** $\mathbf{x}_{\mathbf{actuator}}$ *is available* **then**
16      $\mathbf{x}_{n+1} = \left(\mathbf{M} + \Delta t^2\mathbf{D}^T\mathbf{W}^T\mathbf{W}\mathbf{D}\right)^{-1}$
     $\left(\mathbf{M}\tilde{\mathbf{x}} + \Delta t^2\mathbf{D}^T\mathbf{W}^T\mathbf{W}\left(\mathbf{z}_n - \mathbf{u}_n\right)\right)$
     $+ \mathbb{K}_n\left(\mathbf{y}_n - \hat{\mathbf{y}}_n\right)$ (19)
17   **end**
18 **end**

Output: Position vector of all nodes x.

---

tional error between the simulation and the real exterior points' positions. The whole process described in Fig. 1 forms the proposed KF-ADMM method.

IV. EXPERIMENTAL STUDY AND RESULTS

In this section, the performance of the proposed method is validated in tissue deformation prediction. The open-loop tissue simulator [18] and the closed-loop tissue simulator are compared, and the effect of the size of the marker sets is discussed. The experimental setup shown in Fig. 2 was built. An Aurora electromagnetic (EM) tracker with a Planar 20-20 V2 Field Generator (NDI Europe GmbH, Radolfzell, Germany) was utilized to track the 3D position of a magnetic sensor which was located inside the tissue phantom as shown in Fig. 2. A Vicon motion capture system with five cameras was used to track $4mm$ optic facial markers. Nexus 2.10 software (Vicon Motion Systems, UK) was used to track the markers, and data were transmitted to C++ code using UDP protocol. The proposed method was programmed in C++ using OpenMP, and it was run on an Intel® Core™ i5 processor with 6 cores. Four linear actuators displaced the tissue boundary in discrete steps of $\{5, 10, 15, 20\}$ mm. A tissue phantom made from plastisol and softener (M-F Manufacturing Co, Fort Worth, USA) with an equal volume ratio. The module of elasticity of the phantom that was calculated through
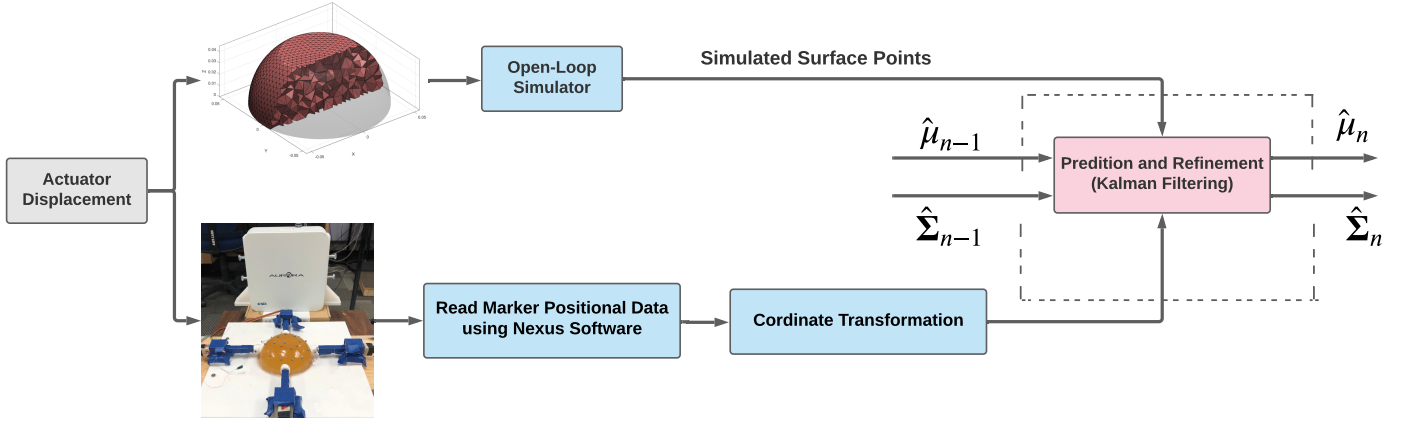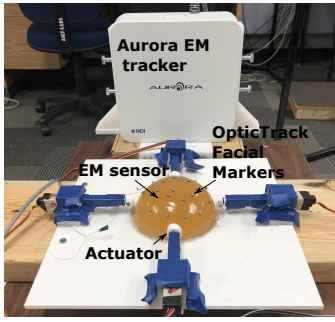
Fig. 1. Flowchart of the proposed KF-ADMM approach.

(a) Setup details including EM sensor, optic markers, phantom and actuators.

(b) The cameras' configuration.

Fig. 2. Experiment setup. An Aurora electromagnetic (EM) tracker is used to track the 3D position of targets. Linear actuators push the tissue phantom made of plastisol. Cameras are used to track facial optic markers mounted on the surface of the phantom.

Fig. 3. The cut view of the mesh with 2331 tetrahedral elements.

for the process noise is set to the value of 3I because of the uncertain nature of the model, and the covariance matrix for the measurement noise is set to the value of 0.01I because the Vicon motion capture system measures with sub-millimeter accuracy.

(a) Marker set 1.   (b) Marker set 2.

Fig. 4. The layout of breast phantom, actuators, targets, and marker set 1 & 2.

compression test is $E = 6$ Kpa. Fig. 3 shows the breast mesh model including 2331 tetrahedral elements. The Tetgen library was used to mesh the CAD model of the barest phantom. Fig. 4 shows the layout of the phantom, the actuators, the target, and the optical markers for the first set, which includes 19 markers, and the second set, which includes 10 markers.

The location of the internal target point, displaced by actuators, was measured for various experiments listed in Table I. The covariance matrices for the model and the measurement noises were chosen with trial and error. The covariance matrix
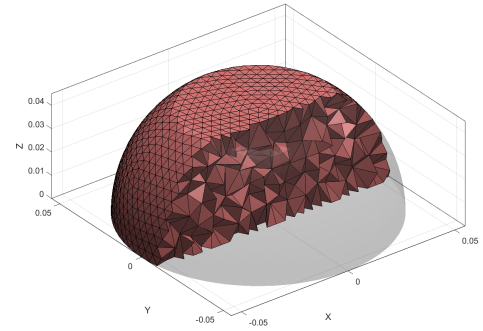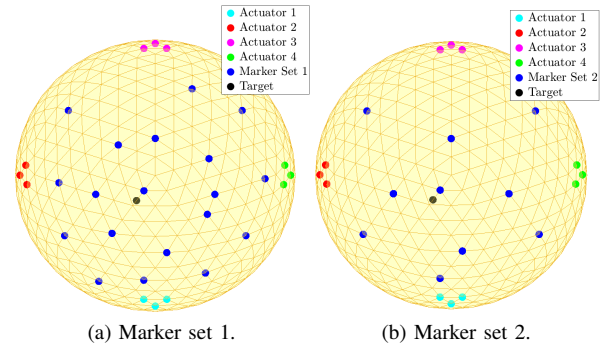
A. Comparison Between the Proposed KF-ADDM Method and the Open-Loop Simulator

To study the effect of the KF-integration on convergence rate, experiments 4, 8, 12, and 16 which have the most deformations are analyzed. The target error, which is the square error between the simulation and experiment results in

the X, Y, and Z directions are plotted against the number of iterations in Fig. 5. Based on the results in Fig. 5, it is evident that convergence happens much faster in the proposed KF-ADMM method. According to Fig. 5, the convergence in the proposed KF-ADMM method is achieved after 200 iterations, while the convergence in the open-loop tissue simulator results occurs after 500 iterations. The open-loop tissue simulator takes 10.58 s to do 500 iterations for 2331 tetrahedral elements while the proposed method takes 7.94 s for 200 iterations for the same number of elements. The computational time can be further improved by implementing the algorithm on GPU; currently, it has been implemented on 6 core CPU. As illustrated in Fig. 5, which represents the target error along the Y-axis, the proposed KF-ADMM method at its final iterations provides a smaller targeting error than that target error provided by an open-loop simulator using ADMM; thus, the accuracy is improved.

B. Analysis of Effect of Marker Set Size

As feedback for the KF-ADMM method, two sets of markers were used to investigate the effect of marker numbers on the accuracy and convergence rate of the KF-ADMM method. A total of 19 markers are included in the first set, and 10 markers are included in the second one (see Fig. 4). The results of the KF-ADMM method using the marker set 1 and 2 are illustrated in Fig. 6. According to Fig. 6, reducing the number of markers increases the target error, though the proposed KF-ADMM with fewer markers still increases the convergence rate and the accuracy compared to ADMM-based open-loop simulation.

The results of the open-loop ADMM and the KF-ADMM using two sets of markers are displayed in Fig. 7. Based on the results represented in Fig. 7, it is found that the KF-ADMM algorithm reduces the mean target error to 0.8 mm while the mean target error of the open-loop simulator is 1.7 mm. By reducing the number of markers, the mean target error of the KF-ADMM increases to 1.1 mm which is still acceptable. The small error of the KF-ADMM method might be due to KF's assumption that model uncertainty is a zero-mean Gaussian noise. As such, KF with the conventional structure cannot compensate for biases.

TABLE I
EXPERIMENTS DESCRIPTION.

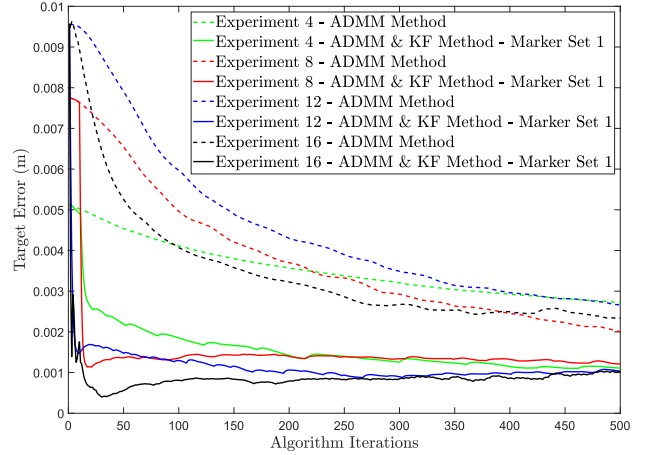| Experiments List		
Experiment Number	Active Actuator	Actuator Movement (mm)
1	1	5
2	1	10
3	1	15
4	1	20
5	2	5
6	2	10
7	2	15
8	2	20
9	1 and 2	5
10	1 and 2	10
11	1 and 2	15
12	1 and 2	20
13	3 and 4	5
14	3 and 4	10
15	3 and 4	15
16	3 and 4	20

Fig. 5. Error target with respect to the number of iterations for the proposed (ADMM KF) and the conventional (ADMM) methods using the first marker set.
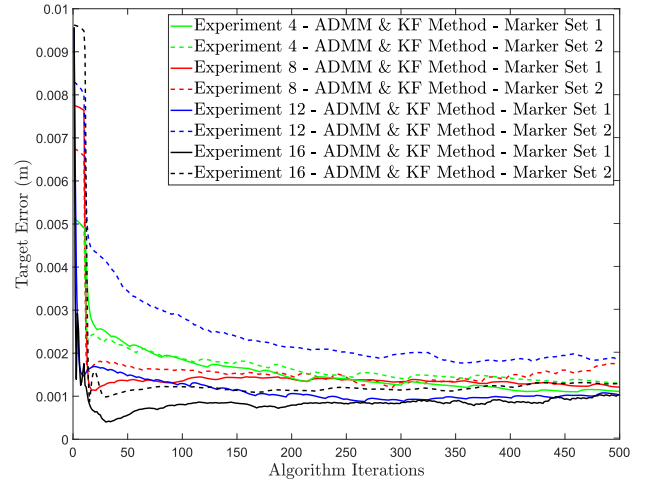

Fig. 6. Error target with respect to the number of iterations for the proposed (ADMM KF) based on the marker set 1 and 2.
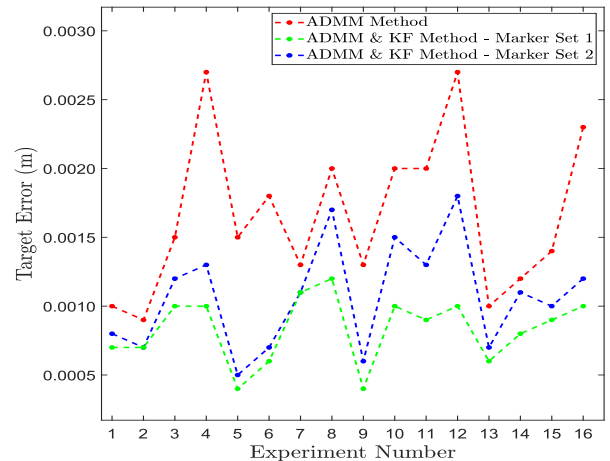

Fig. 7. Comparison between the accuracy of the proposed and the conventional method for 16 experiments.

V. Conclusion and Discussion

In this paper, a new method called KF-ADMM is introduced to improve the performance of the open-loop deformable object simulator (ADMM-based projective dynamics method). To simulate tissue deformation, the dynamics of soft tissue were turned into a parallelizable optimization problem. In the KF-ADMM method, a Kalman filter is incorporated into the ADMM-based projective dynamics to improve the modeling accuracy by updating the position of internal nodes based on the surface node positional measurements. This data is easily obtained by using optic markers or the Kinect sensor. The accuracy of the proposed approach was evaluated by carrying out several experimental studies on a breast tissue phantom.

The intended application of the proposed KF-ADMM method is in breast brachytherapy; however, the proposed method can be implemented in any other applications in which a biomechanical model of the tissue is required. The advantages of the proposed KF-ADMM over the open-loop simulator are:

1) The KF-ADMM models the nonlinear mechanical behavior (e.g., hyperelasticity), and the experimental results were in agreement with the model's prediction.

2) Because the KF-ADMM solution is parallelizable, this solver is an ideal choice for real-time computer-assisted surgery applications.

3) The proposed algorithm improved the accuracy of the deformation prediction by 52% on average. Based on the obtained results, the improvement is more pronounced when tissue is extremely deformed.

4) The required iterations to reach convergence are reduced with the proposed KF-ADMM method. KF calculation will add extra computations to the algorithm but because the required number of iterations is reduced significantly compared to the open-loop tissue simulator, the overall computation time is reduced while the accuracy is improved.

The effect of unmodeled dynamics terms are considered as zero-mean Gaussian distribution, which is a limiting assumption considering the nonlinearity of tissue dynamics. This assumption results in a small mean targeting error of the KF-ADMM method. To eliminate the remnant error, a non-Gaussian noise model with non-zero mean can be used to account for the effect of unmodelled dynamics terms. Currently, the proposed framework cannot handle markers failure, as the loss of data can result in accuracy reduction. KF structure can be improved to allow for measurement dropouts.

References

[1] W. Liu, J. Carriere, T. Meyer, R. Sloboda, S. Husain, N. Usmani, Z. Yang, and M. Tavakoli, "Intraoperative optimization of seed implantation plan in breast brachytherapy," *International Journal of Computer Assisted Radiology and Surgery*, vol. 16, no. 6, pp. 1027–1035, 2021.

[2] E. E. Deurloo, K. G. Gilhuijs, L. J. S. Kool, and S. H. Muller, "Displacement of breast tissue and needle deviations during stereotactic procedures," *Investigative radiology*, vol. 36, no. 6, pp. 347–353, 2001.

[3] J. op den Buijs, M. Abayazid, C. L. de Korte, and S. Misra, "Target motion predictions for pre-operative planning during needle-based interventions," in *2011 Annual International Conference of the IEEE Engineering in Medicine and Biology Society*. IEEE, 2011, pp. 5380–5385.

[4] J. Michael, D. Morton, D. Batchelar, M. Hilts, J. Crook, and A. Fenster, "Development of a 3d ultrasound guidance system for permanent breast seed implantation," *Medical Physics*, vol. 45, no. 8, pp. 3481–3495, 2018.

[5] U. Meier, O. López, C. Monserrat, M. C. Juan, and M. Alcaniz, "Real-time deformable models for surgery simulation: a survey," *Computer methods and programs in biomedicine*, vol. 77, no. 3, pp. 183–197, 2005.

[6] J. Zhang, Y. Zhong, and C. Gu, "Deformable models for surgical simulation: a survey," *IEEE reviews in biomedical engineering*, vol. 11, pp. 143–164, 2017.

[7] N. Lauzeral, D. Borzacchiello, M. Kugler, D. George, Y. Rémond, A. Hostettler, and F. Chinesta, "A model order reduction approach to create patient-specific mechanical models of human liver in computational medicine applications," *Computer methods and programs in biomedicine*, vol. 170, pp. 95–106, 2019.

[8] J. de Jesús Rubio, "Stability analysis of the modified levenberg–marquardt algorithm for the artificial neural network training," *IEEE transactions on neural networks and learning systems*, vol. 32, no. 8, pp. 3510–3524, 2020.

[9] J. de Jesús Rubio, M. A. Islas, G. Ochoa, D. R. Cruz, E. Garcia, and J. Pacheco, "Convergent newton method and neural network for the electric energy usage prediction," *Information Sciences*, vol. 585, pp. 89–112, 2022.

[10] A. Mendizabal, E. Tagliabue, J.-N. Brunet, D. Dall'Alba, P. Fiorini, and S. Cotin, "Physics-based deep neural network for real-time lesion tracking in ultrasound-guided breast biopsy," in *Computational Biomechanics for Medicine*. Springer, 2019, pp. 33–45.

[11] Y. Duan, W. Huang, H. Chang, W. Chen, J. Zhou, S. K. Teo, Y. Su, C. K. Chui, and S. Chang, "Volume preserved mass–spring model with novel constraints for soft tissue deformation," *IEEE journal of biomedical and health informatics*, vol. 20, no. 1, pp. 268–280, 2014.

[12] G. San-Vicente, I. Aguinaga, and J. T. Celigueta, "Cubical mass-spring model design based on a tensile deformation test and nonlinear material model," *IEEE Transactions on Visualization and Computer Graphics*, vol. 18, no. 2, pp. 228–241, 2011.

[13] E. Basafa and F. Farahmand, "Real-time simulation of the nonlinear visco-elastic deformations of soft tissues," *International journal of computer assisted radiology and surgery*, vol. 6, no. 3, pp. 297–307, 2011.

[14] I. Berndt, R. Torchelsen, and A. Maciel, "Efficient surgical cutting with position-based dynamics," *IEEE computer graphics and applications*, vol. 37, no. 3, pp. 24–31, 2017.

[15] M. Müller, B. Heidelberger, M. Hennix, and J. Ratcliff, "Position based dynamics," *Journal of Visual Communication and Image Representation*, vol. 18, no. 2, pp. 109–118, 2007.

[16] E. Tagliabue, D. Dall'Alba, E. Magnabosco, C. Tenga, I. Peterlík, and P. Fiorini, "Position-based modeling of lesion displacement in ultrasound-guided breast biopsy," *International journal of computer assisted radiology and surgery*, vol. 14, no. 8, pp. 1329–1339, 2019.

[17] S. Bouaziz, S. Martin, T. Liu, L. Kavan, and M. Pauly, "Projective dynamics: fusing constraint projections for fast simulation," *ACM Transactions on Graphics (TOG)*, vol. 33, no. 4, pp. 1–11, 2014.

[18] M. Overby, G. E. Brown, J. Li, and R. Narain, "Admm : Projective dynamics: Fast simulation of hyperelastic models with dynamic constraints," *IEEE Transactions on Visualization and Computer Graphics*, vol. 23, no. 10, pp. 2222–2234, 2017.

[19] M. C. Yip, D. G. Lowe, S. E. Salcudean, R. N. Rohling, and C. Y. Nguan, "Tissue tracking and registration for image-guided surgery," *IEEE transactions on medical imaging*, vol. 31, no. 11, pp. 2169–2182, 2012.

[20] J. Song, J. Wang, L. Zhao, S. Huang, and G. Dissanayake, "Dynamic reconstruction of deformable soft-tissue with stereo scope in minimal invasive surgery," *IEEE Robotics and Automation Letters*, vol. 3, no. 1, pp. 155–162, 2017.

[21] F. Liu, Z. Li, Y. Han, J. Lu, F. Richter, and M. C. Yip, "Real-to-sim registration of deformable soft tissue with position-based dynamics for surgical robot autonomy," in *2021 IEEE International Conference on Robotics and Automation (ICRA)*. IEEE, 2021, pp. 12 328–12 334.

[22] S. Boyd, N. Parikh, and E. Chu, *Distributed optimization and statistical learning via the alternating direction method of multipliers*. Now Publishers Inc, 2011.

[23] E. W. Chaves, *Notes on continuum mechanics*. Springer Science & Business Media, 2013.

[24] A. Samani, J. Zubovits, and D. Plewes, "Elastic moduli of normal and pathological human breast tissues: an inversion-technique-based

investigation of 169 samples," *Physics in medicine & biology*, vol. 52, no. 6, p. 1565, 2007.

[25] J. Bonet and R. D. Wood, *Nonlinear continuum mechanics for finite element analysis*. Cambridge university press, 1997.

Ron S.Sloboda received the B.Sc. degree in physics from the University of Manitoba, Winnipeg, MB, Canada, in 1974, and the Ph.D. degree in physics, nuclear theory, from the University of Alberta, Edmonton, AB, Canada, in 1979. He is currently a Professor in the Department of Oncology, University of Alberta. His research interests include dosimetry and treatment planning for brachytherapy, including the design of clinical studies to obtain patient data and model based dose calculation.

Mehrnoosh Afshar received the BSc degree in mechanical engineering from Amirkabir University of Technology (Tehran Polytechnic) in 2014 and the MSc degree in mechanical engineering from the Sharif University of Technology in 2016. She is currently pursuing a Ph.D. in Electrical Engineering at the University of Alberta. Her research interests involve mechanical design, modeling and application of theory of control in medical application. Currently, she focuses on developing systems for Robot-assisted breast brachytherapy.

Nawaid Usmani main focus on research is in prostate brachytherapy. Dr. Usmani's main objective for this research is to characterize current brachytherapy techniques and identify strategies for improving this treatment. In addition to this research in prostate brachytherapy, Dr. Usmani is involved in a number of other research endeavours. His other research includes: Investigating the potential benefits of metformin in preventing metabolic complications of hormonal therapy and improving prostate cancer outcomes; Identifying new prognostic or predictive biomarkers in prostate cancer; Investigating the utility of magnetic resonant imaging and PET imaging in the management of prostate cancer; and Investigating the potential benefits of exercise in rectal cancer patients.

Jay Carriere earned his B.Sc. in Electrical Engineering and Ph.D. in Biomedical Engineering from the University of Alberta, Alberta, Canada in 2011 and 2019, respectively. He was a Post-Doctoral Research Fellow in the Department of Electrical and Computer Engineering at the University of Alberta and currently he is an assistant professor at university of Calgary. His research interests involve medical robotics, medical image processing, imageguided robotic-assisted surgery, and collaborative robotics.

Siraj Hussain Husain completed medical school at the Dalhousie University (Halifax, Nova Scotia) followed by residency training at the University of Alberta (Edmonton, Alberta). He completed a fellowship in Radiation Oncology at the University of Western Ontario (London, Ontario). His current clinical areas of focus include genitourinary and breast cancer. He has clinical and research interests in Brachytherapy and leads the implementation and training of HDR to new physicians at the Tom Baker Cancer Centre (TBCC). Dr. Husain is the Clinical and Research Program Leader for Prostate Brachytherapy, Radiation Oncology, at the TBCC. Active areas of research include enhancement and progression of combined modality therapy (Prostate Brachy + External Beam Radiation Therapy), champion for intermediate and high risk prostate cancer "drafted protocol" for introduction of High Dose Rate (HDR) and research, continue to advocate for Breast Brachytherapy – with new research project to enhance and improve the procedure.

Hossein Rouhani is an Associate Professor in the Department of Mechanical Engineering at the University of Alberta, and a Research Affiliate at the Glenrose Rehabilitation Hospital (Edmonton). He is also the founder and director of Neuromuscular Control Biomechanical Laboratory. He received an MSc degree in Mechanical Engineering from the University of Tehran, Iran, and a PhD degree in Biotechnology and Bioengineering from the Swiss Federal Institute of Technology in Lausanne (EPFL).

Tyler Meyer Meyer is now a medical physicist at the Tom Baker Cancer Centre in Calgary. He is also an adjunct associate professor at the U of C in the department of oncology, with a secondary appointment in the department of physics and astronomy. The primary focus of his research and clinical practice is brachytherapy, a classification of radiotherapy where radioactive seeds or sources are placed in or near the target area. It's commonly used in cancer treatment for prostate, cervical and other gynecological cancers. But Meyer is also doing groundbreaking research on breast brachytherapy.

Mahdi Tavakoli is a Professor in the Department of Electrical and Computer Engineering, University of Alberta, Canada. He received his BSc and MSc degrees in Electrical Engineering from Ferdowsi University and K.N. Toosi University, Iran, in 1996 and 1999, respectively. He received his PhD degree in Electrical and Computer Engineering from the University of Western Ontario, Canada, in 2005. In 2006, he was a post-doctoral researcher at Canadian Surgical Technologies and Advanced Robotics (CSTAR), Canada. In 2007-2008, he was an NSERC Post-Doctoral Fellow at Harvard University, USA. Dr. Tavakoli's research interests broadly involve the areas of robotics and systems control. Specifically, his research focuses on haptics and teleoperation control, medical robotics, and image-guided surgery. Dr. Tavakoli is the lead author of Haptics for Teleoperated Surgical Robotic Systems (World Scientific, 2008). He is a Senior Member of IEEE and an Associate Editor for IEEE/ASME Transactions on Mechatronics, Journal of Medical Robotics Research, IET Control Theory Applications, and Mechatronics.